Electronic Supplementary Information

Direct synthesis of multiple heteroatoms functionalized mesoporous silica adsorbents from phosphate industry mining byproducts. Decontaminating water from Pb(II) ions as an application case.

Ali Mohammed Yimer[a], Ayalew H. Assen[a,*], Hamid Ait Said[b], Abdessamad Elamri[a,c], Omar Lakbita[a], Anthony Rousseau[c], Karim Adil[a,c], Hicham Benyoucef[a,b], Youssef Daafi[d], Youssef Belmabkhout[a,*]

[a]Applied Chemistry and Engineering Research Centre of Excellence (ACER CoE), Mohammed VI Polytechnic University (UM6P), Lot 660 - Hay Moulay Rachid, 43150 Ben Guerir, Morocco

[b]High Throughput Multidisciplinary Research Laboratory (HTMR), Mohammed VI Polytechnic University (UM6P), Lot 660 - Hay Moulay Rachid, 43150 Ben Guerir, Morocco

[c]Le Mans Université, Institut des Molécules et des Matériaux du Mans (UMR 6283), Avenue Olivier Messiaen, 72085 Le Mans Cedex, France

[d] Office Chérifien des Phosphates (OCP) group, Strategic Business Unit (SBU) Mining, 2-4, Rue Al Abtal, Hay Erraha 20200, Maroc-BP Maârif 5196, Casablanca, Morocco

*Corresponding authors: A. H. Assen (Email: ayalew.assen@um6p.ma); Y. Belmabkhout (E-mail: youssef.belmabkhout@um6p.ma)

1. Characterization Methods

A variety of analytical techniques were employed to characterize the synthesized hetero-functional MSM sorbents.

Powder X-ray diffraction (PXRD) data were collected in monochromator mode over the 2θ range 5−80° and parallel plate mode for the 2θ range 0−5°on an XRDynamic 500 Automated multipurpose diffractometer (Anton Paar) using Cu-Kα radiation (λ = 1.54056 Å, 50 kV/340 mA) with a step size of 0.005° in 2θ.

Thermal characteristics were investigated through thermogravimetric analysis (TGA) in the temperature range of 25 to 800 °C, employing an SDTQ600 TA instrument with a controlled heating rate of 5°C/min under airflow.

Inductively coupled plasma optical emission spectrometry (ICP-OES) was conducted using Agilent 5110 instrument to determine the chemical compositions of the PMWs and MSM frameworks and determine the Pb(II) adsorption capacities of the synthesized adsorbents.

Fourier Transform Infrared Spectroscopy (FT-IR) measurements were performed using an Alpha II Bruker spectrometer in ATR (Attenuated Total Reflectance) sampling mode, in the range of 4000 - 400 cm^{-1} at a resolution of 4 cm^{-1}, with 64 scans.

Surface morphology was examined via scanning electron microscopy combined with energy-dispersive X-ray analysis (SEM-EDX). The sample analysis was conducted using a TESCAN TIMA scanning electron microscope. Samples were prepared and mounted on aluminum stubs using conductive carbon tape. The integrated energy-dispersive X-ray spectroscopy (EDX) system enabled quantitative elemental analysis.

Transmission electron microscope (TEM) images were taken by a JEOL JEM-2100 at an accelerating voltage of 200 kV with a LaB6 source and equipped with a Gatan Ultra scan camera. The JEOL JEM-2100 is also equipped with JED 2300T energy dispersive X-ray spectrometer (EDX) system and allows the elemental analysis of samples. The samples were prepared by depositing a drop of sonicated material onto a 300-mesh carbon-coated copper grid and allowing it to air dry overnight.

Chemical compositions of the phosphate mining waste (PMW) precursors were examined by X-ray fluorescence (XRF) analysis. The sample analysis was conducted using a Rigaku EDXRF (Energy Dispersive X-ray Fluorescence) spectrometer.

N_2 sorption experiments at 77 K were conducted using a 3-Flex Surface Characterization Analyzer (Micromeritics), covering relative pressures up to 1 bar. The cryogenic temperature for N_2 sorption was regulated using a liquid nitrogen bath at 77 K. Specific surface areas were calculated by applying the Brunauer-Emmett-Teller (BET) model to the N_2 adsorption isotherms collected at 77 K. Pore size analyses were performed using the Barrett-Joyner-Halenda (BJH) pore model system for each mesoporous silicates from the adsorption branches. Prior to N_2 sorption measurements, both the PMWs precursors (PMW1 and PMW2) and the prepared PMWs-based mesoporous materials (PMW1-MSM1, PMW1-MSM2, PMW2-MSM3, and PMW2-MSM4) samples were degassed under vacuum at 150 °C for 12 h.

Room temperature water vapor adsorption isotherms were obtained using a Vstar1 vapor sorption analyzer (Quantachrome instrument), with activated (guest-free) samples, and a constant manifold temperature of 110 °C was maintained throughout the procedure.

The zeta potential of the developed adsorbents was determined using a Zeta-sizer (Nano ZS90, Malvern Ltd.). 5 mg of the powder (0.05 wt%) was dispersed in 10 mL of KCl (1 mM). The pH (3–11) of the suspensions was adjusted using HCl (0.1 M) or NaOH (0.1 M) solutions, and the samples were sonicated for 30 min. 1 mL of the sample was poured into a cuvette, and its surface charge was measured. The zeta potential of MSMs was also measured after Pb^{2+} (1500 mg/L) removal.

2. Supplementary Figures and Notes

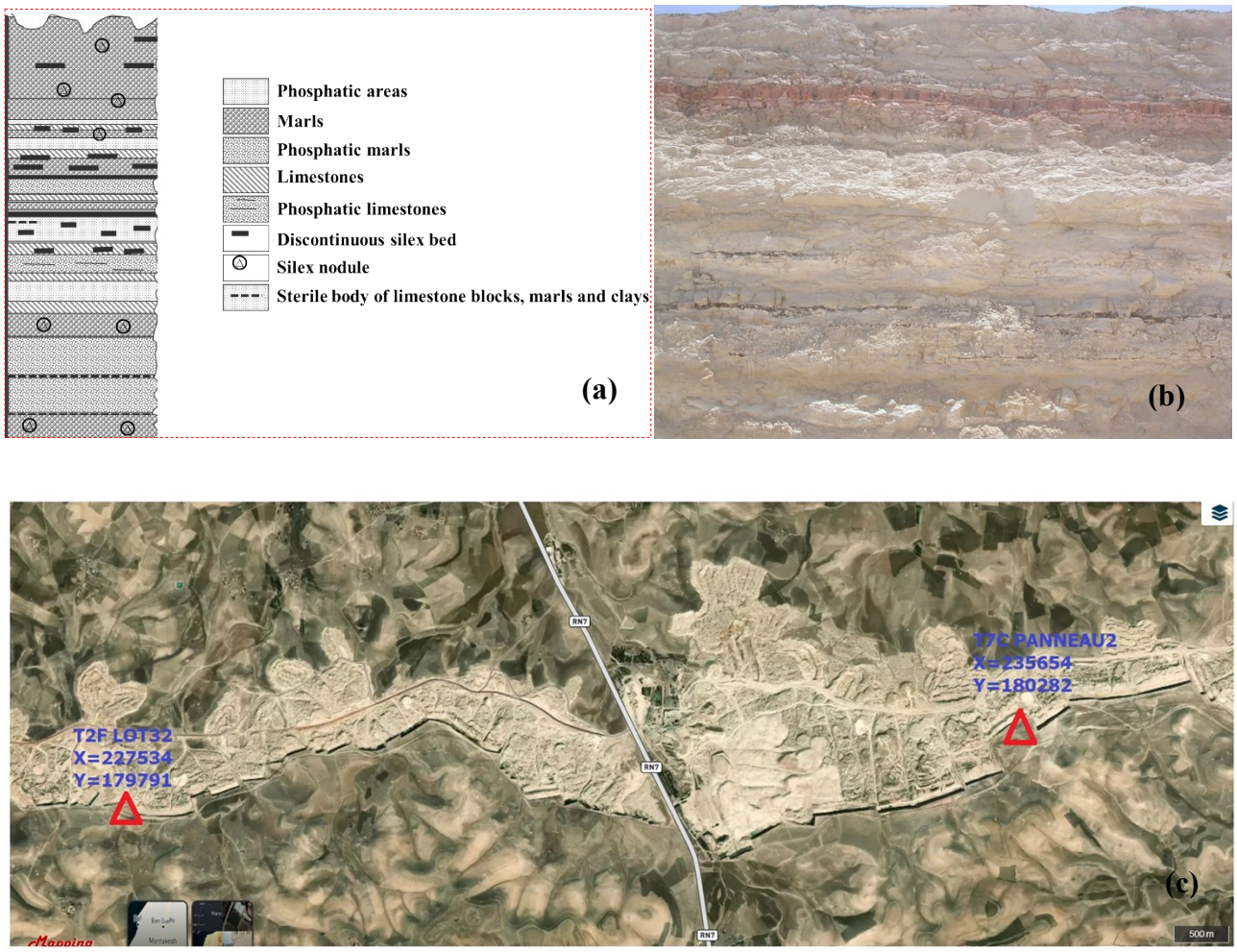

Fig. S1. A general illustration of Moroccan phosphate ore deposit and the different waste rock interlayers that can be separated from the phosphate during mining or extraction operation (a); Photograph showing an actual geological cross-section of a working face in the Youssoufia mine, showing the position of the red clay layer in relation to the layer level (phosphate and non-phosphate) (b); and the location of the Youssoufia mining waste rock landfill sites where the waste samples were collected (c).

Note: In the phosphate extraction operations of the Youssoufia region in Morocco, a comprehensive understanding of the geological and operational aspects is crucial. The region is notable for its open pit mining methods, specifically targeting phosphate ores interlayered with various types of waste rocks, including the notable red clays from the Ypresian age, as depicted in the photograph provided in Fig. S1b. The extraction process begins with the removal of the overburden, a non-phosphatic layer composed of topsoil and other surface materials. This initial step is essential to expose the phosphate

ore beds beneath. Once the overburden is cleared, the mining operation proceeds to the extraction of phosphate-rich strata, which are characteristically sub-horizontal and interspersed with layers of limestone, marls, and clays (Fig. S1). These layers vary significantly in thickness and composition, which presents a unique challenge in terms of material handling and processing. During the extraction phase, the phosphate ore is often accompanied by significant quantities of gangue materials, including flintstone, sand, and residual phosphate minerals. To effectively manage this, the ore undergoes primary crushing, a process designed to reduce the size of the extracted material to facilitate subsequent handling and processing steps. The crushed ore is then sieved to separate finer phosphate particles from larger waste rock fragments. This sieving process produces different categories of waste rock, including destoning waste from particles larger than 60 mm and screening waste from particles larger than 10 mm. The resulting waste materials from these processes are diverse in composition, comprising clays, limestones, marls, and residual phosphate. Managing this waste is a complex task, requiring advanced sorting and valorization techniques to minimize environmental impact and enhance resource utilization. One promising approach involves the use of ore sorting technologies that can effectively separate valuable phosphate minerals from the waste matrix based on their physical and chemical properties.

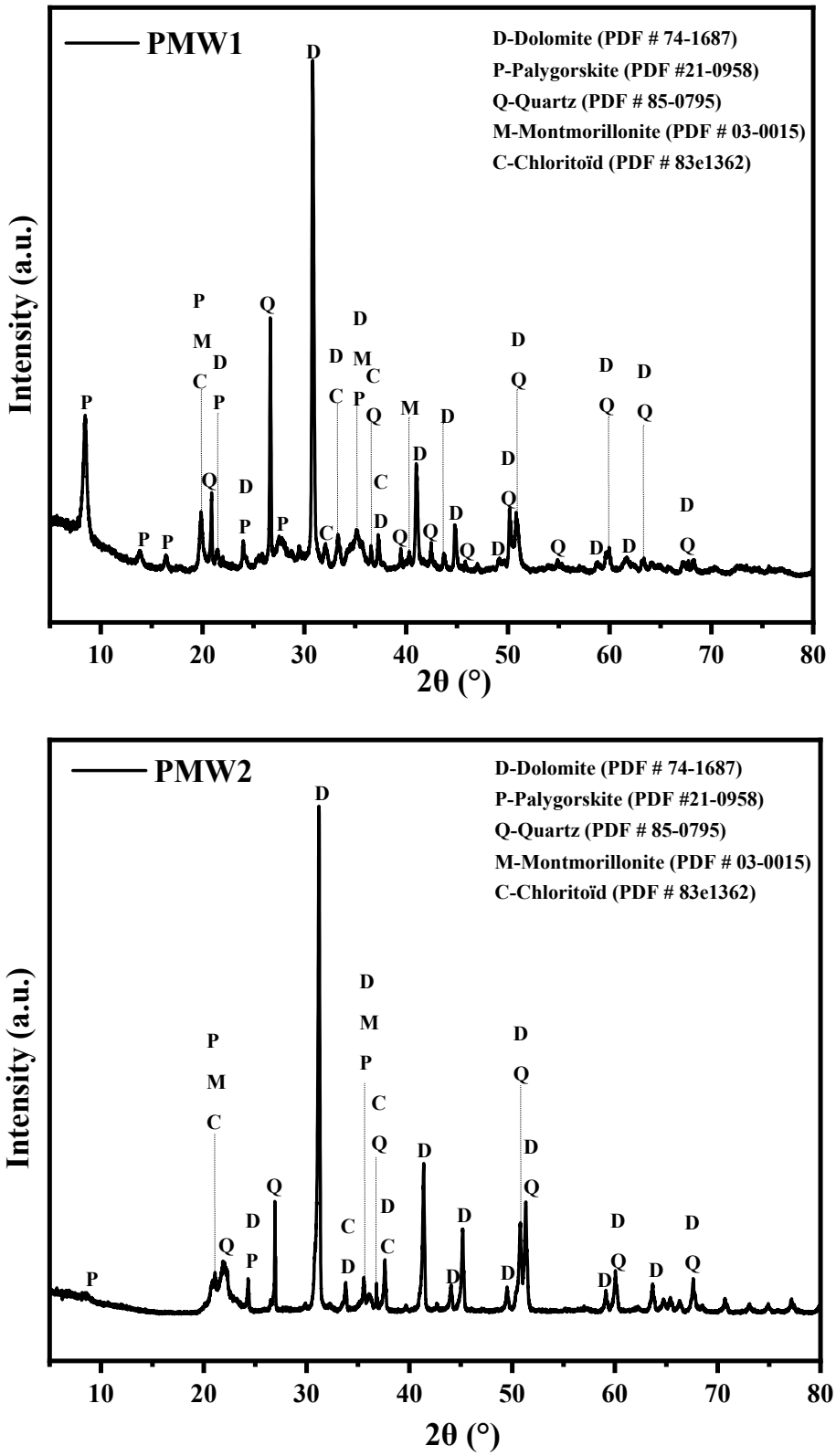

Fig. S2. XRD patterns of Red-PMW or PMW1 (Top)Yellow-PMW or PMW2(Bottom).

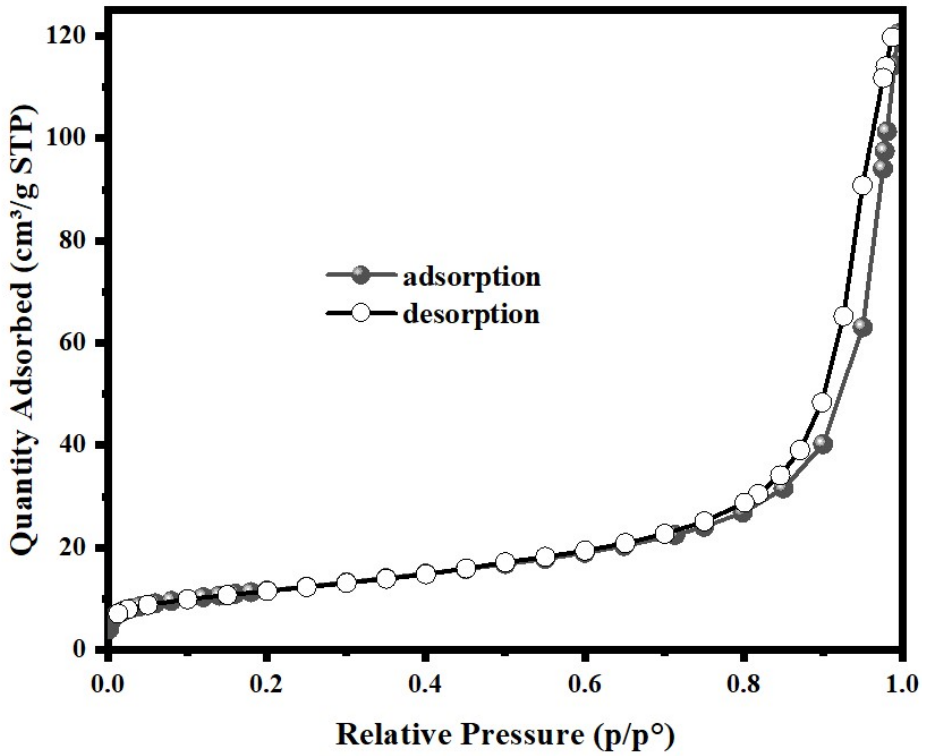

Fig. S3. N_2 adsorption-desorption isotherm of Red-PMW or PMW1 collected at 77 K.

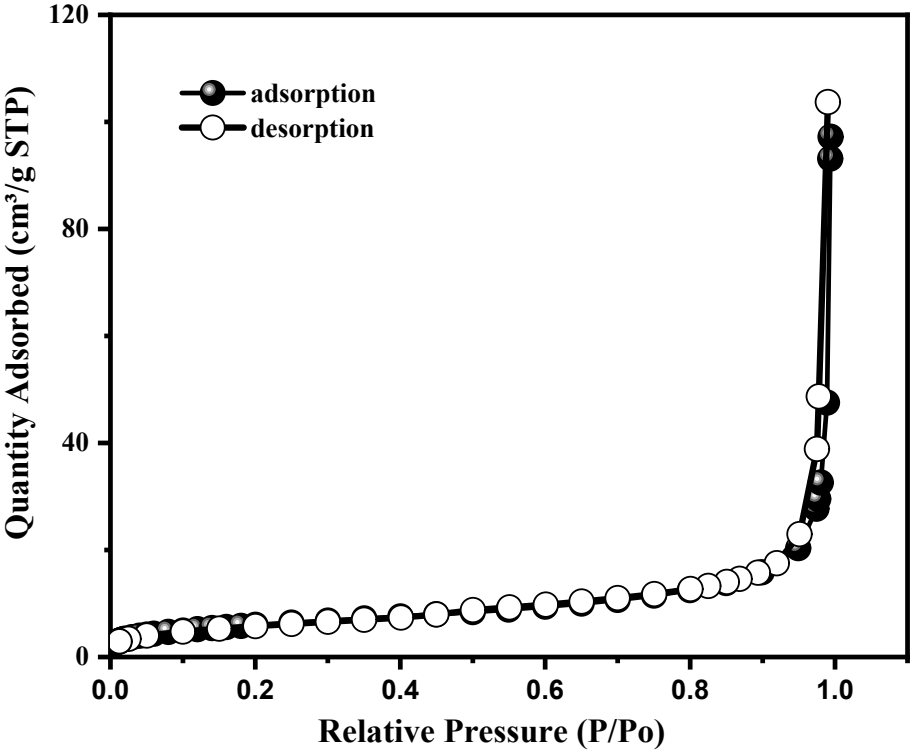

Fig. S4. N_2 adsorption-desorption isotherm of Yellow-PMW or PMW collected at 77 K.

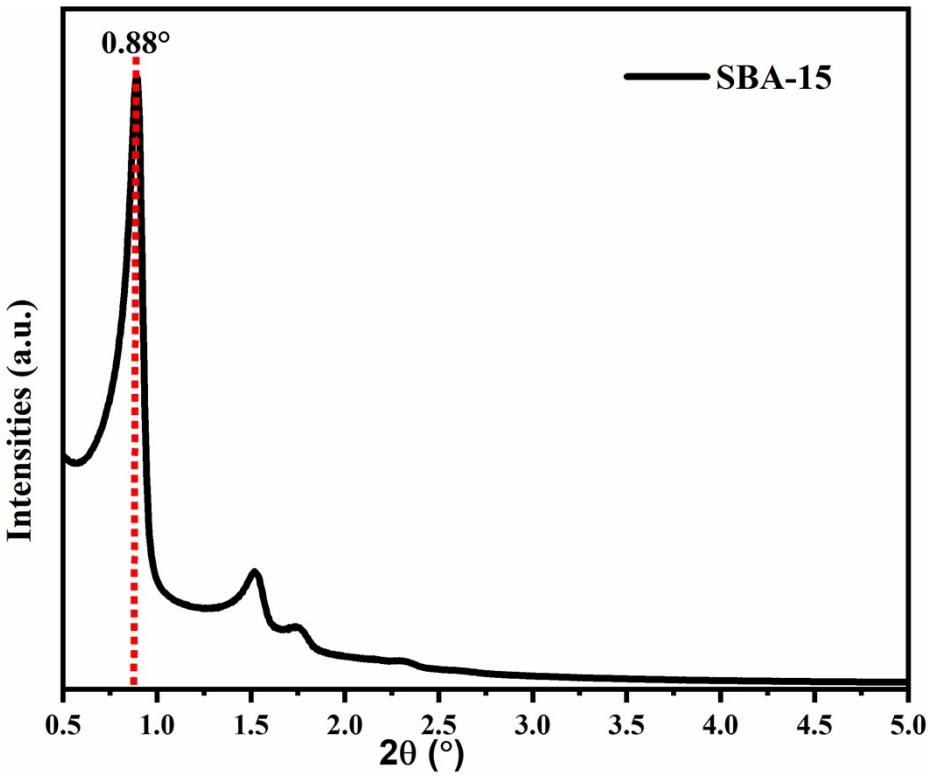

Fig. S5. Small-angle XRD analysis of SBA-15

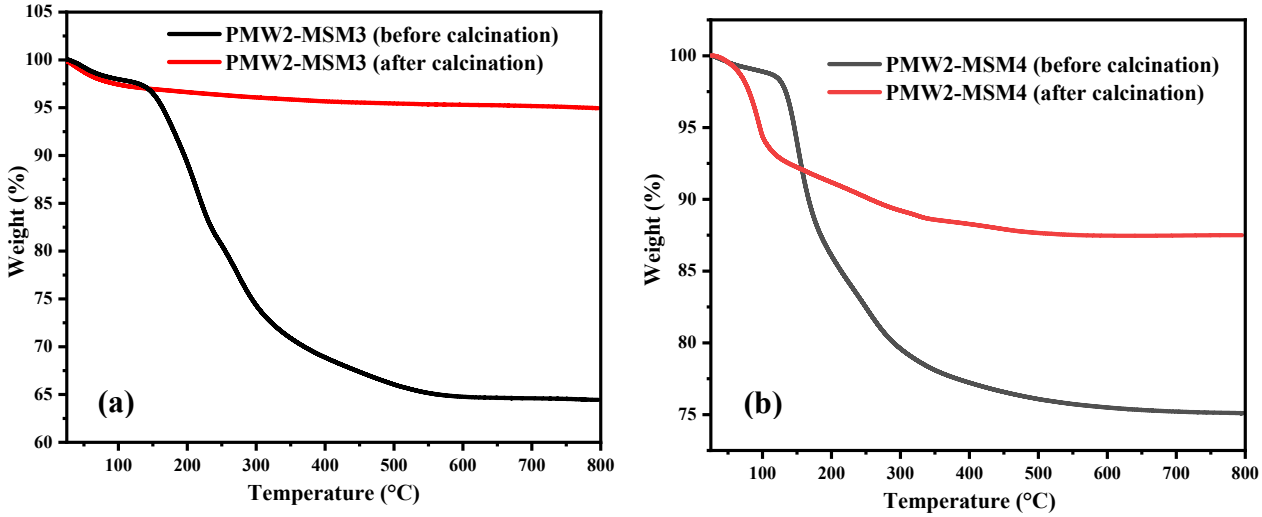

Fig. S6 TGA analysis for PMW2-MSM3 (**a**) and PMW2-MSM4 (**b**).

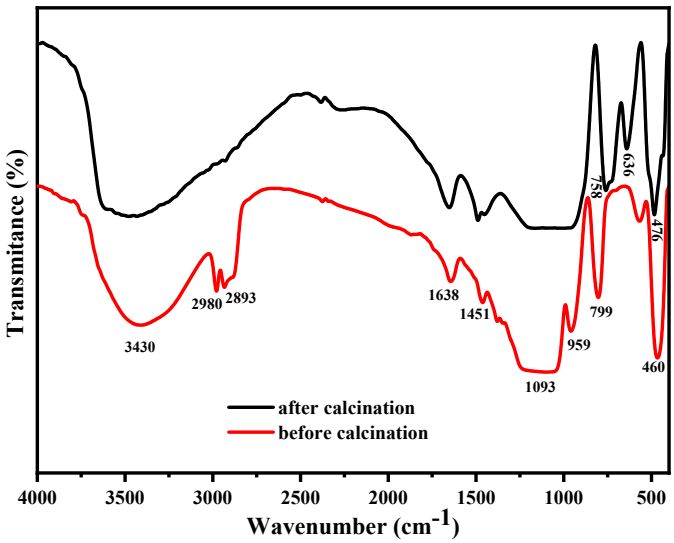

Fig. S7 FTIR analysis of PMW1-MSM1

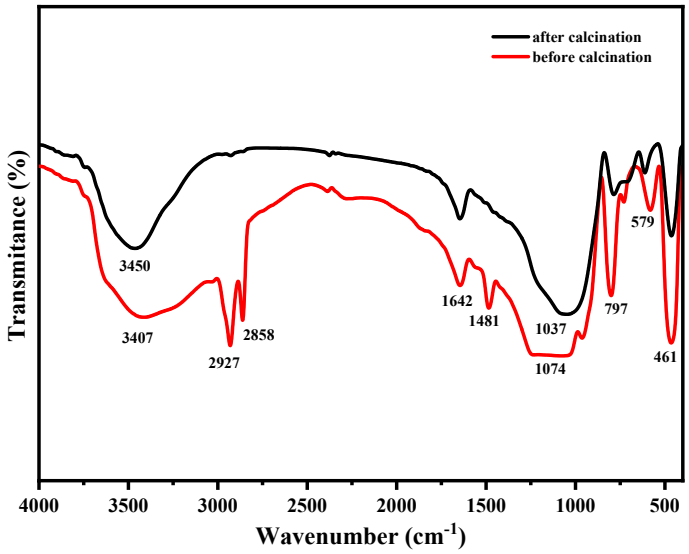

Fig. S8 FTIR analysis of PMW1-MSM2

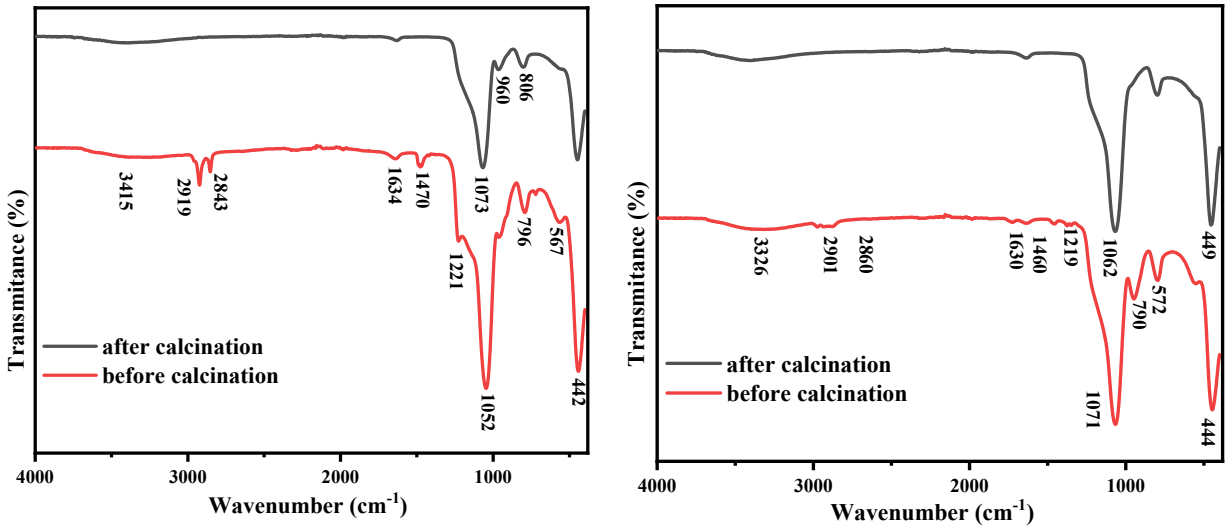

Fig. S9 FTIR analysis of PMW2-MSM3 (Left) and PMW2-MSM4 (Right).

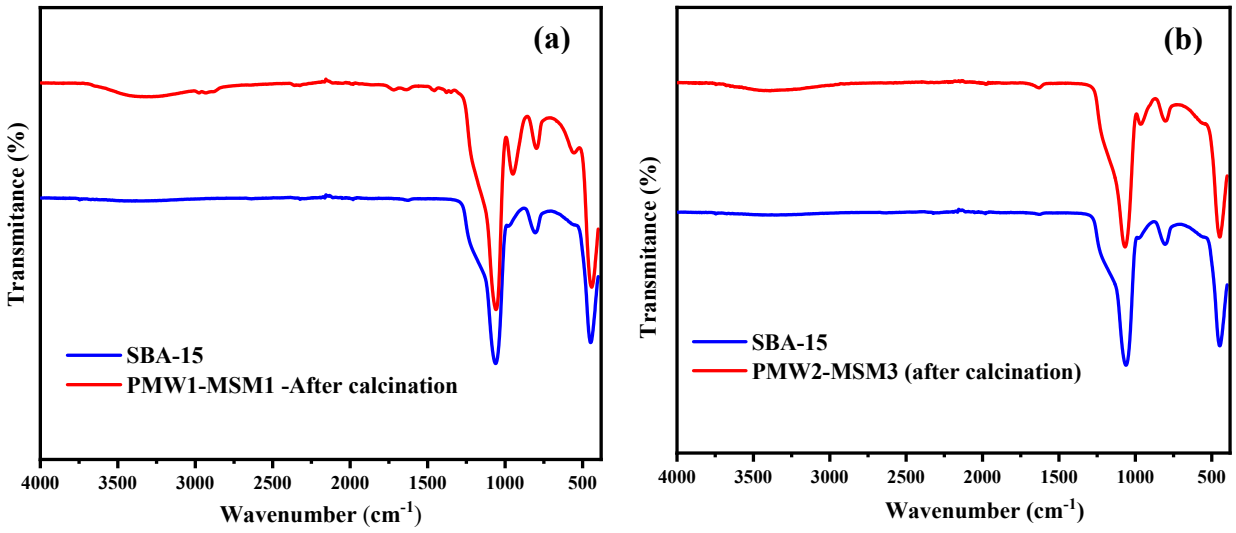

Fig. S10. Comparison of FTIR data with commercial SBA-15: (a) PMW1-MSM1 and (**b**) PMW2-MSM3 and SBA-15 (**b**).

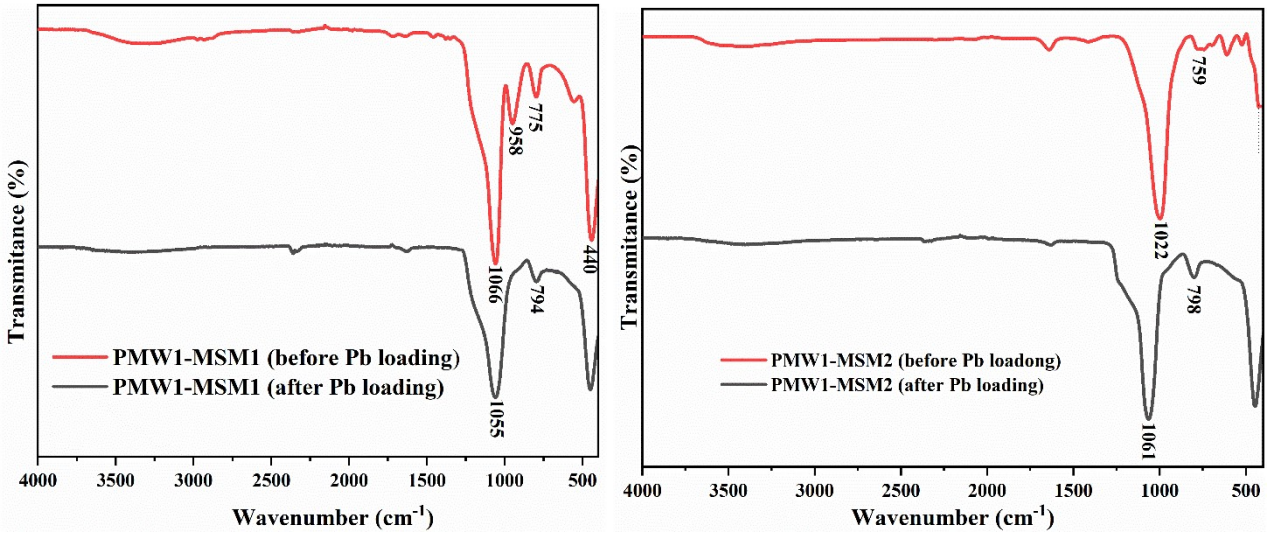

Fig. S11 Comparison of FTIR data with commercial SBA-15: (a) PMW1-MSM1 and (**b**) PMW2-MSM3 and SBA-15 (**b**).

(i)

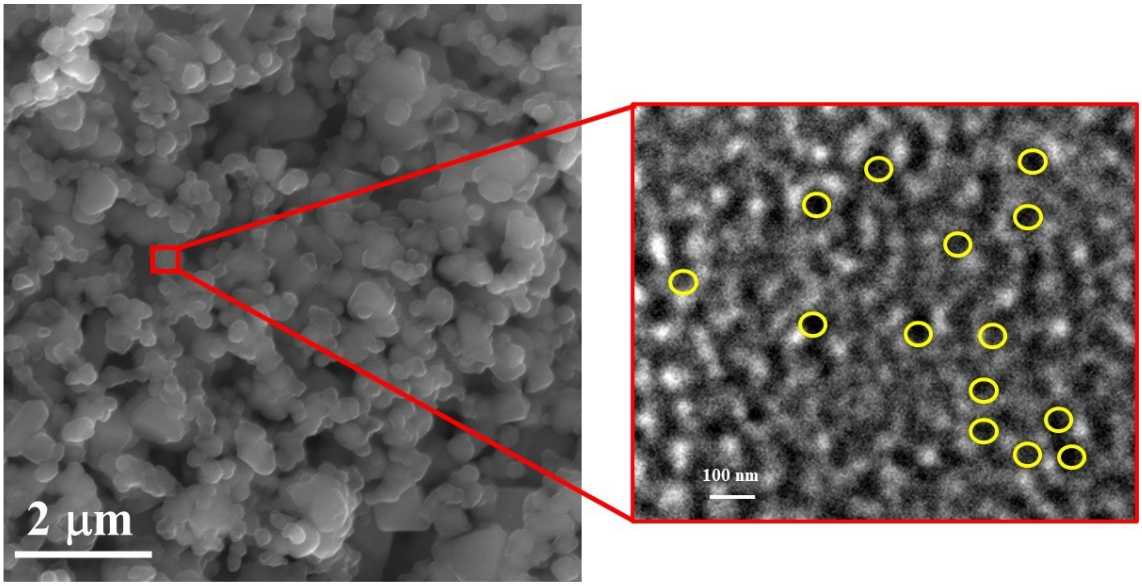

(ii)

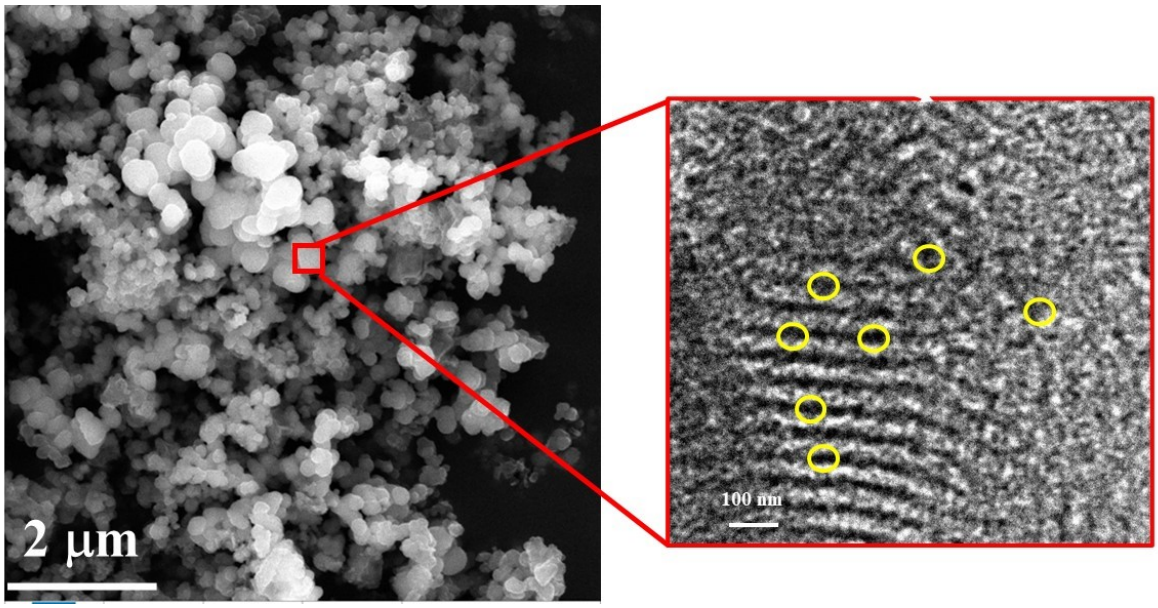

Fig. S12. SEM image of (i) PMW1-MSM1 alongside a TEM image to characterize its porosity and (ii) PMW1-MSM2 alongside a TEM image to characterize its porosity.

(i)

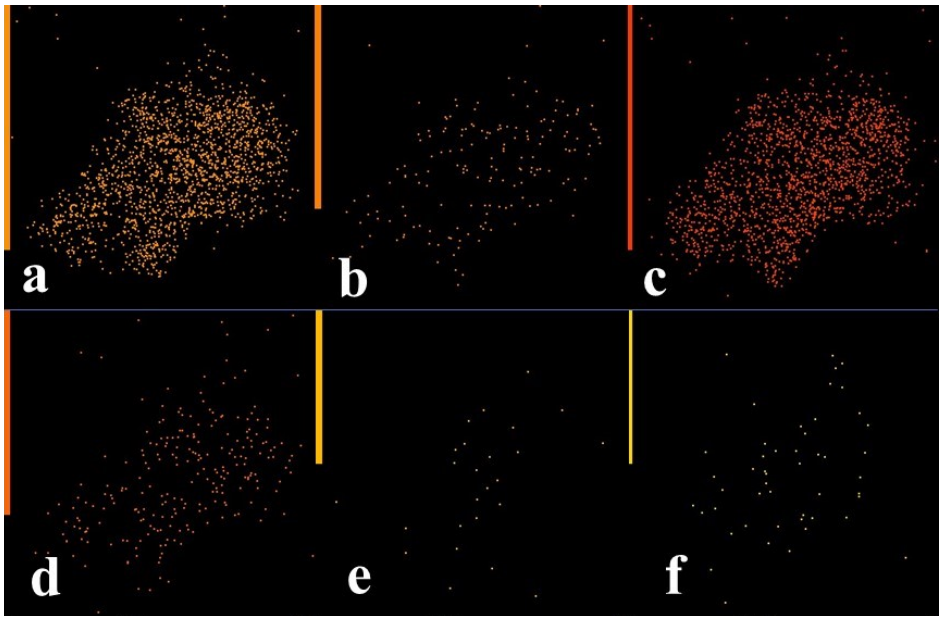

(ii)

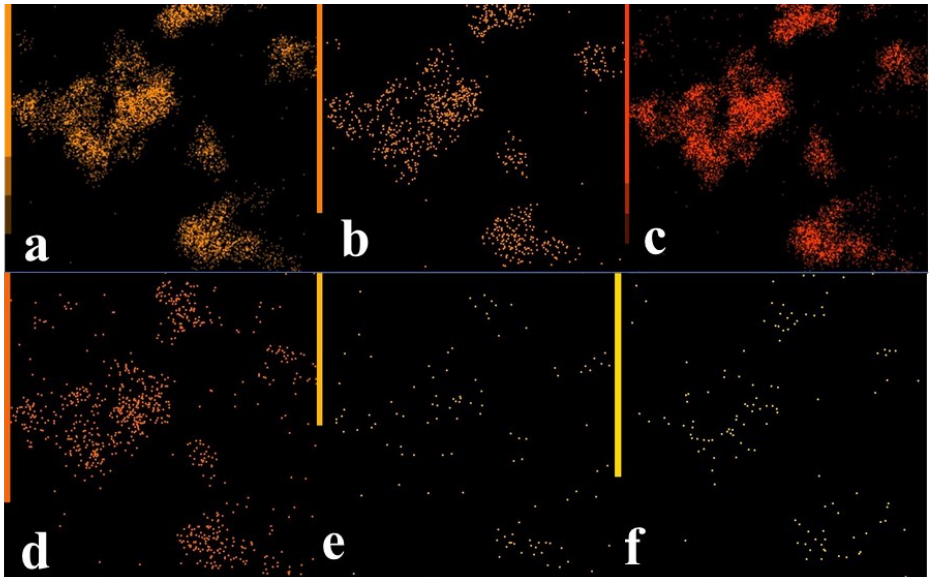

Fig. S13 TEM-EDX maps of (i) PMW1-MSM1 ((a) Si; (b) Al; (c) O; (d) Na (e) Cl and (e) K) and (ii) PMW1-MSM2 ((a) Si; (b) Al; (c) O; (d) Na (e) Cl and (e) K) [size of scale bar = 2.0 μm].

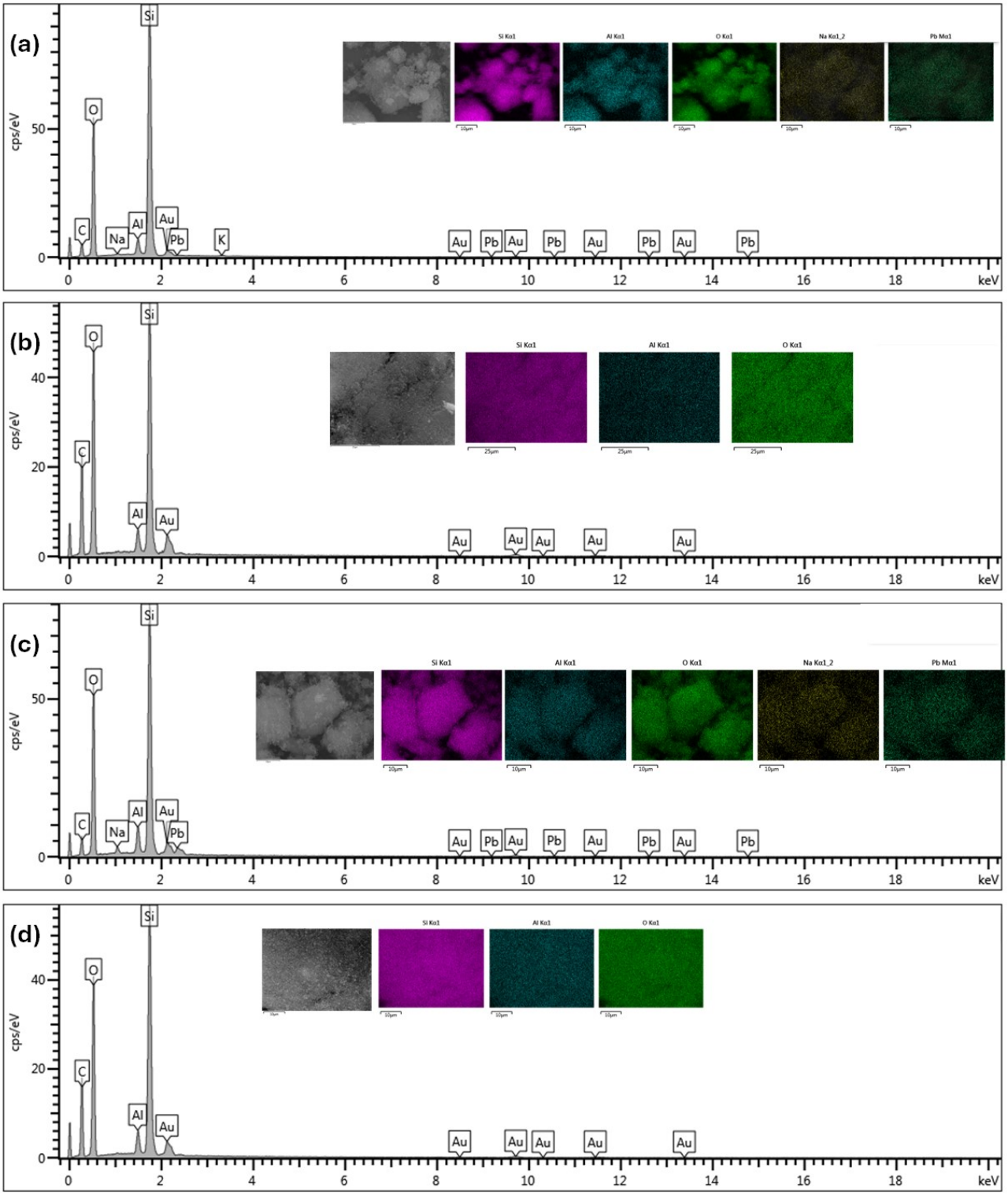

Fig. S14 SEM-EDX analysis of PMW1-MSM1 after Pb(II) adsorption (a), PMW1-MSM1 after four Pb(II) adsorption-desorption cycles (b); PMW1-MSM2 after Pb(II) adsorption (c), PMW1-MSM2 after four Pb(II) adsorption-desorption cycles (d).

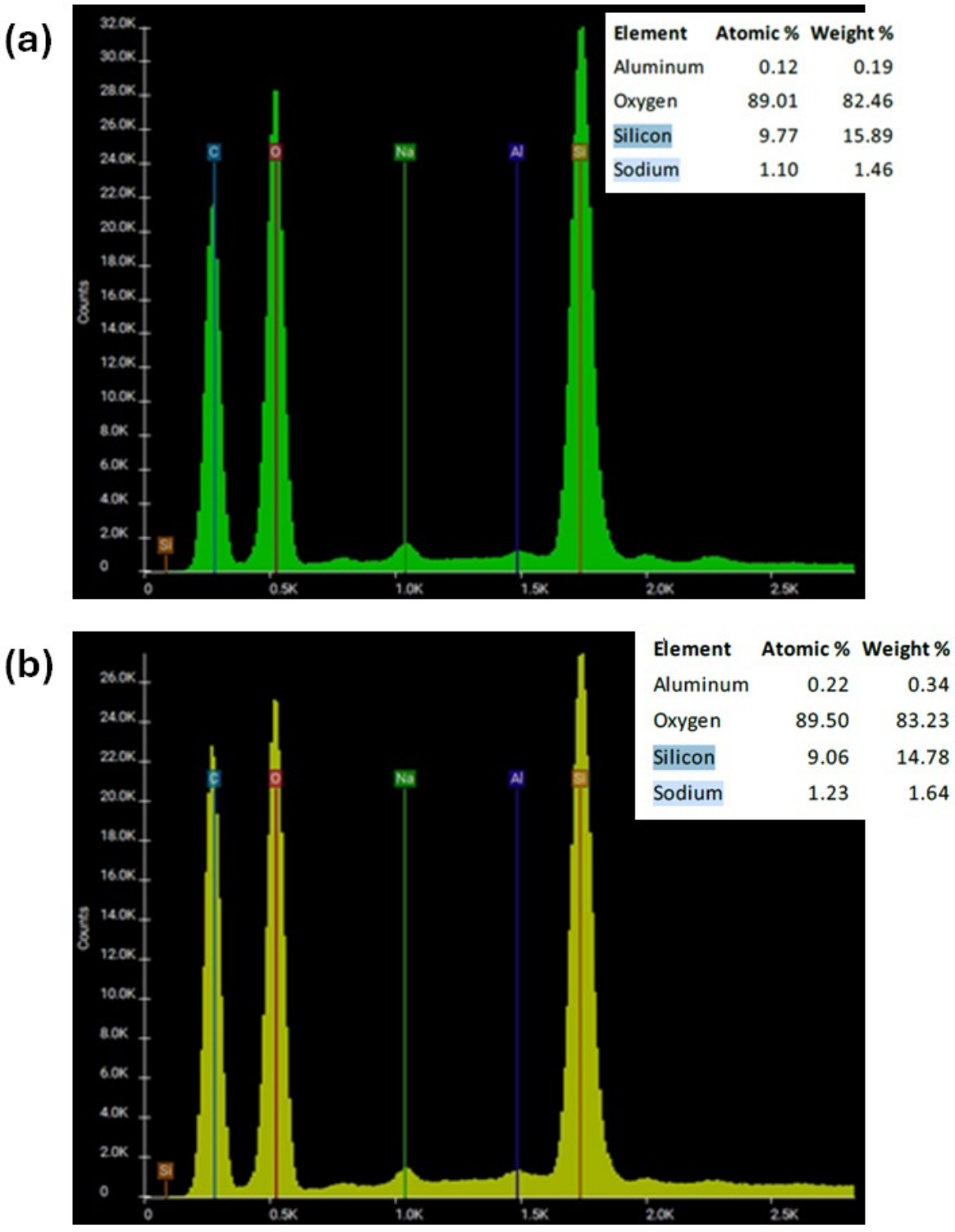

Fig. S15. Comparison of the EDX spectra of PMW1-MSM1 before (a) PMW1-MSM2 (b) before lead adsorption.

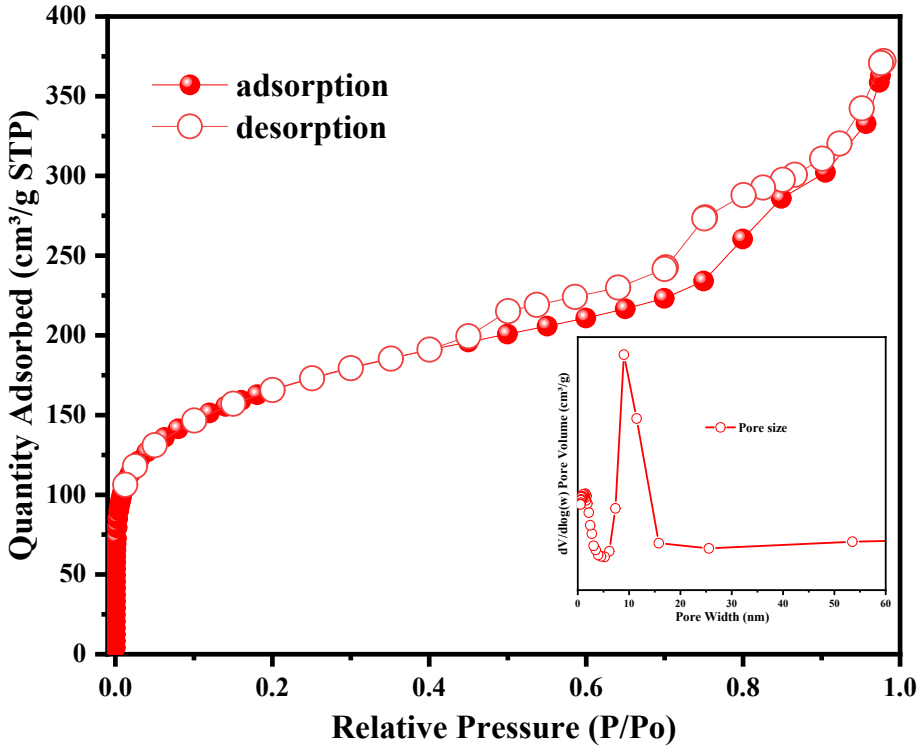

Fig S16: N_2 adsorption-desorption isotherms for PMW2-MSM3

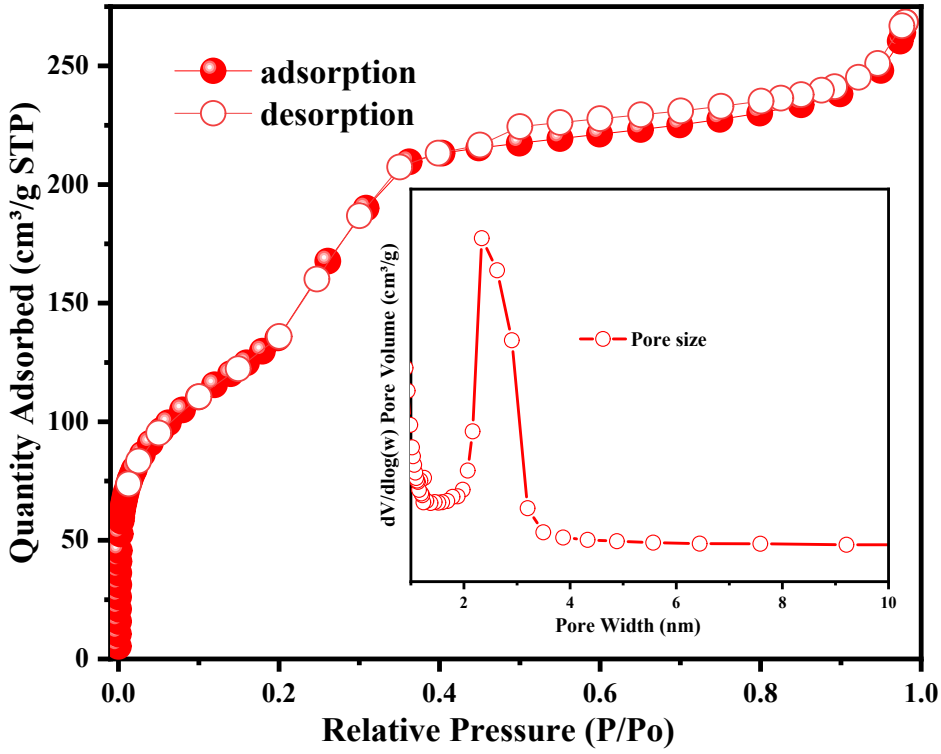

Fig S17: N_2 adsorption-desorption isotherms for PMW2-MSM4.

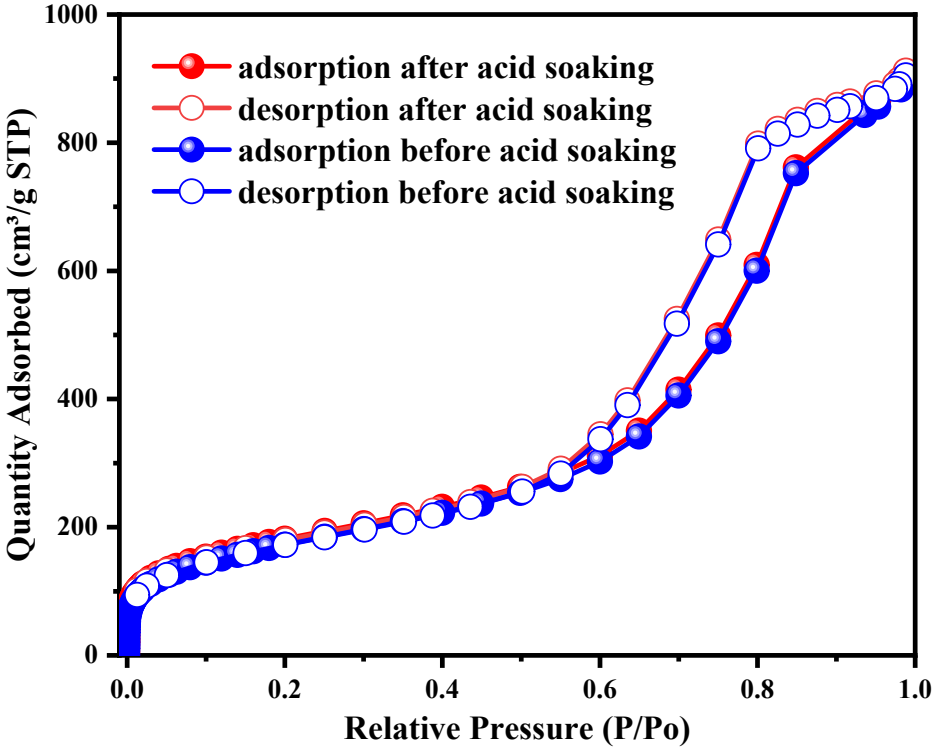

Fig. S18. N_2 adsorption-desorption isotherms for PMW1-MSM1 before and after HCl soaking

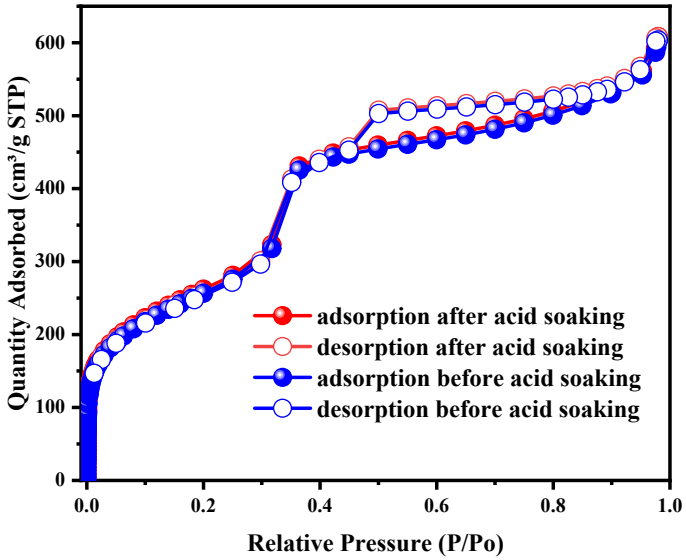

Fig. S19. N_2 adsorption-desorption isotherms for PMW1-MSM2 before and after HCl soaking.

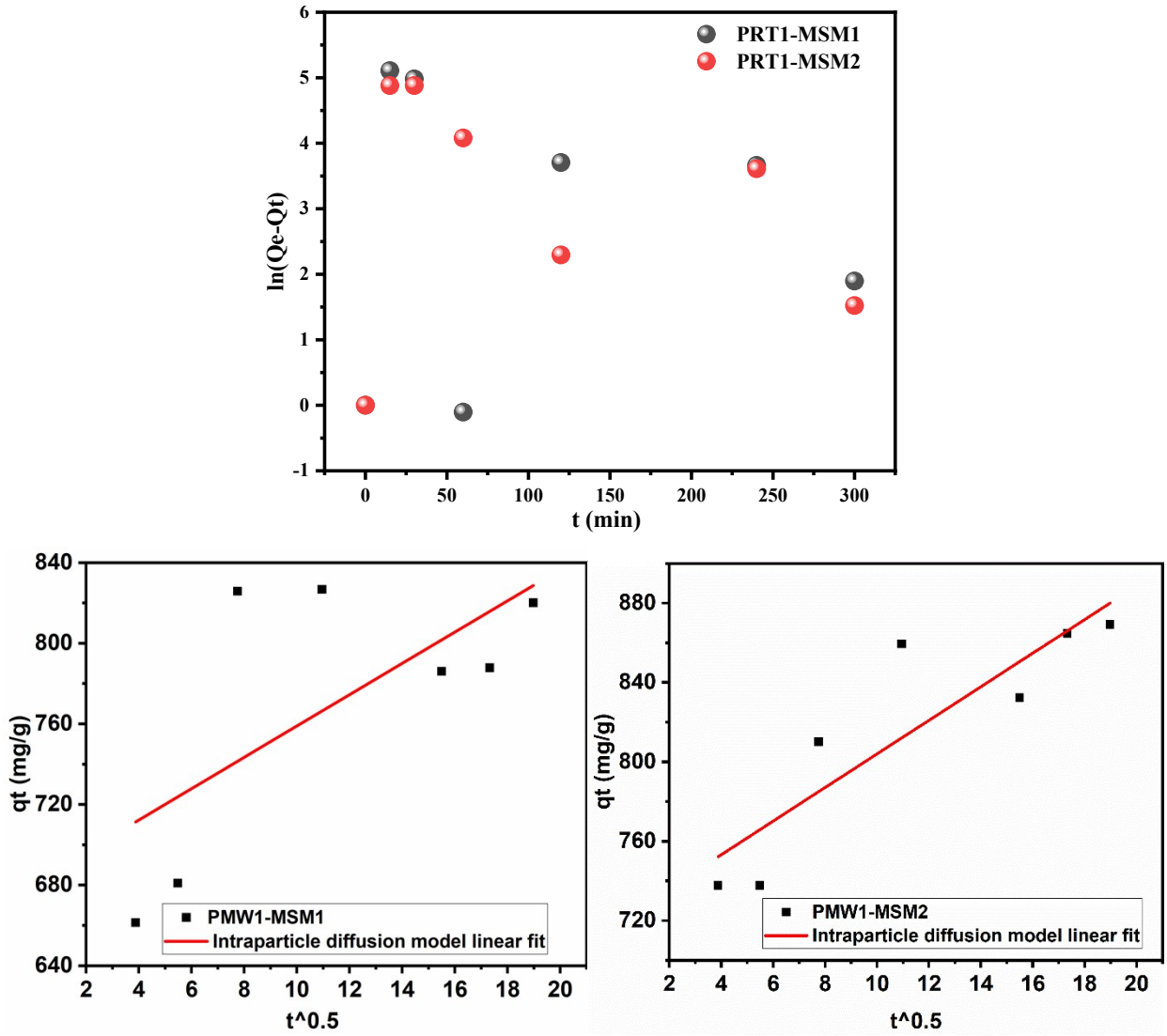

Fig. S20. Adsorption kinetics models: Pseudo-first-order model fitting plots of Pb^{2+} adsorption onto MSMs (Top) and Intraparticle diffusion sorption plot of Pb(II) on PMW1-MSM1 (Bottom left), and PMW1-MSM2 (Bottom right).

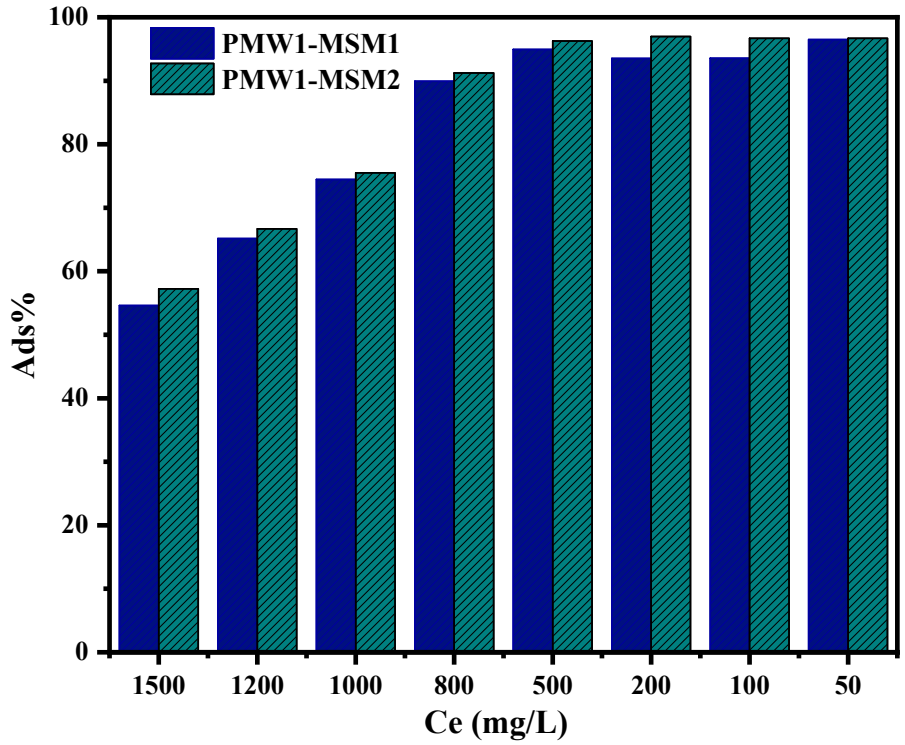

Fig. S21. Percent removal efficiency of Pb(II) by the synthesized MSMs.

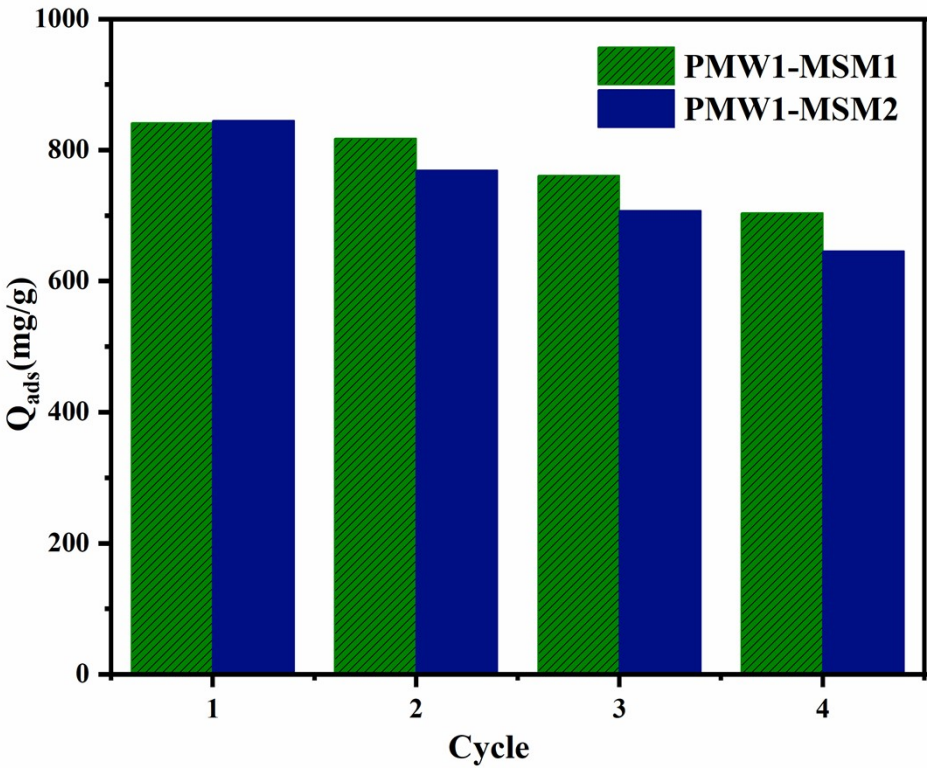

Fig. S22. Reusability of Pb^{2+} adsorption onto MSMs.

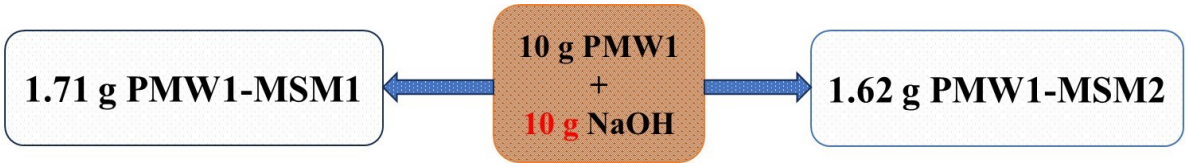

Fig. S23. Mass balance of PMW1-MSMs synthesis from 10 g of PMW1 and 10 g NaOH. It is assumed that about 5.85 and 6.17 kg NaOH is required to prepare 1 kg of PMW1-MSM1 and PMW1-MSM2, respectively.

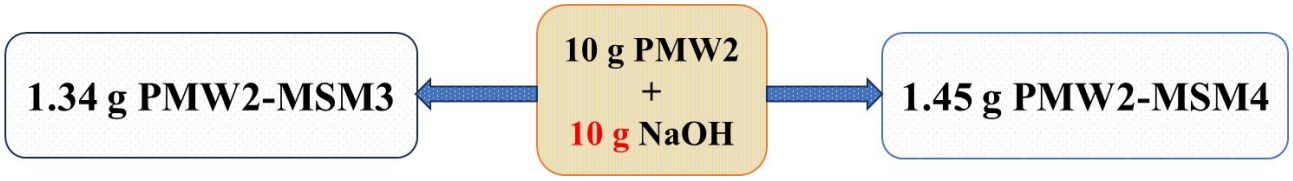

Fig. S24. Mass balance of PMW2-MSMs synthesis from 10 g of PMW2 and 10 g NaOH.

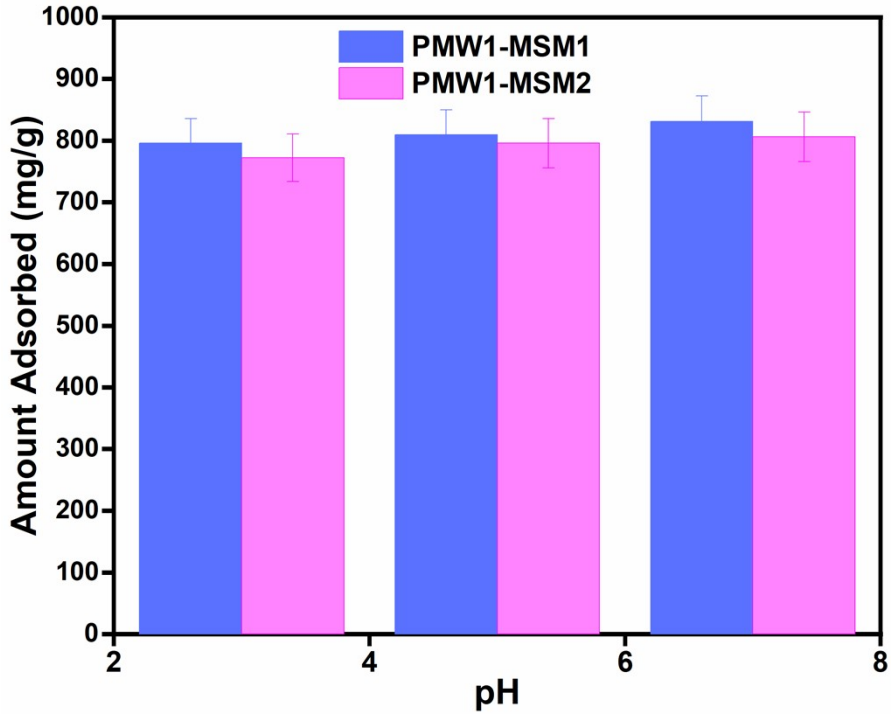

Fig. S25. Effect of pH on the adsorption performance of Pb(II) by the adsorbents with a 2 h contact time, 100 mg/L Pb^{2+} concentration, 25 mg adsorbent dosage, and at 25 °C.

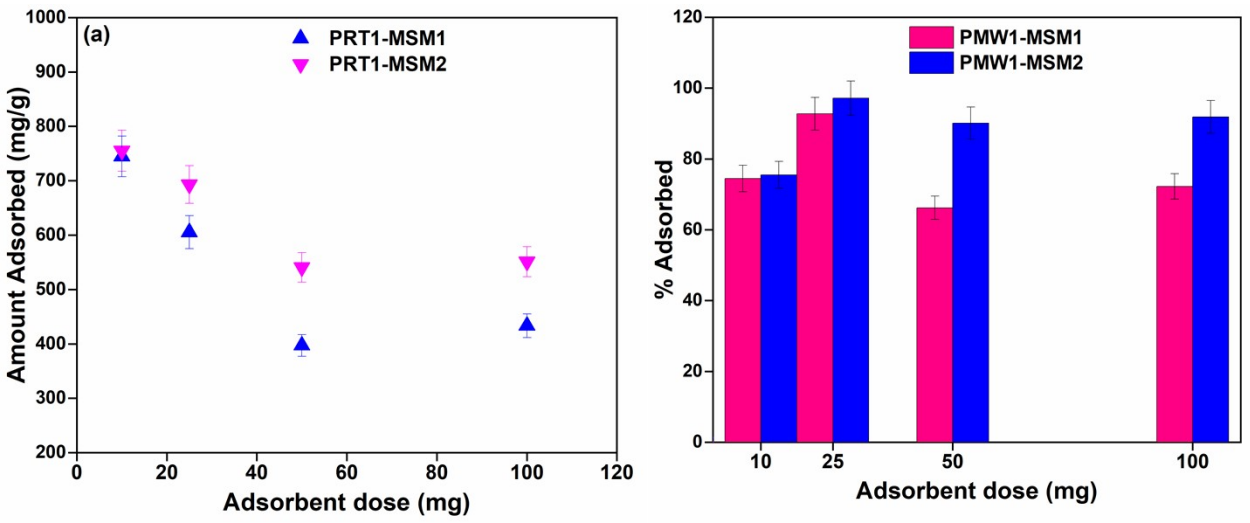

Fig. S26. The effect of adsorbent dosage assessed using 1000 mg/L lead solution at pH 5 and 2 h incubation time.

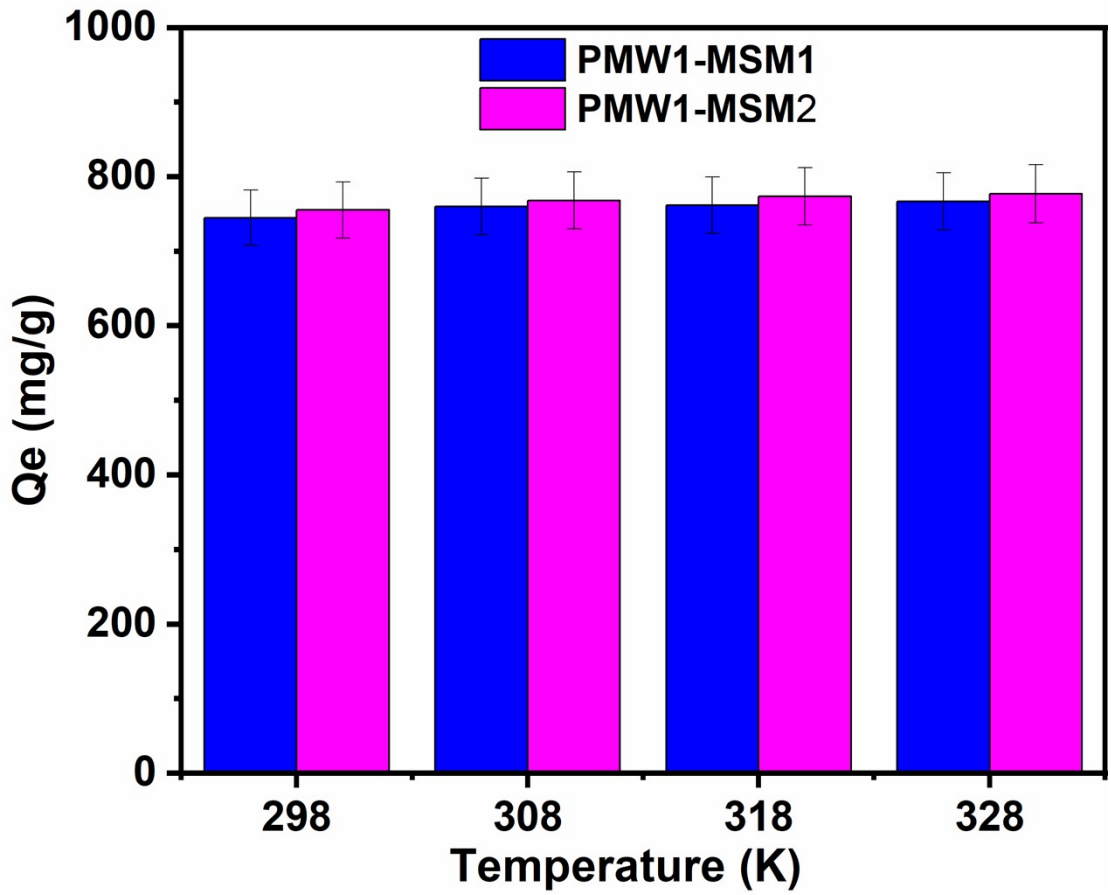

Fig. S27. The effect of temperature on Pb(II) adsorption capacity assessed using 25 mg adsorbent dose, 2 h contact time, and 100 mg/L lead solution at pH 5.

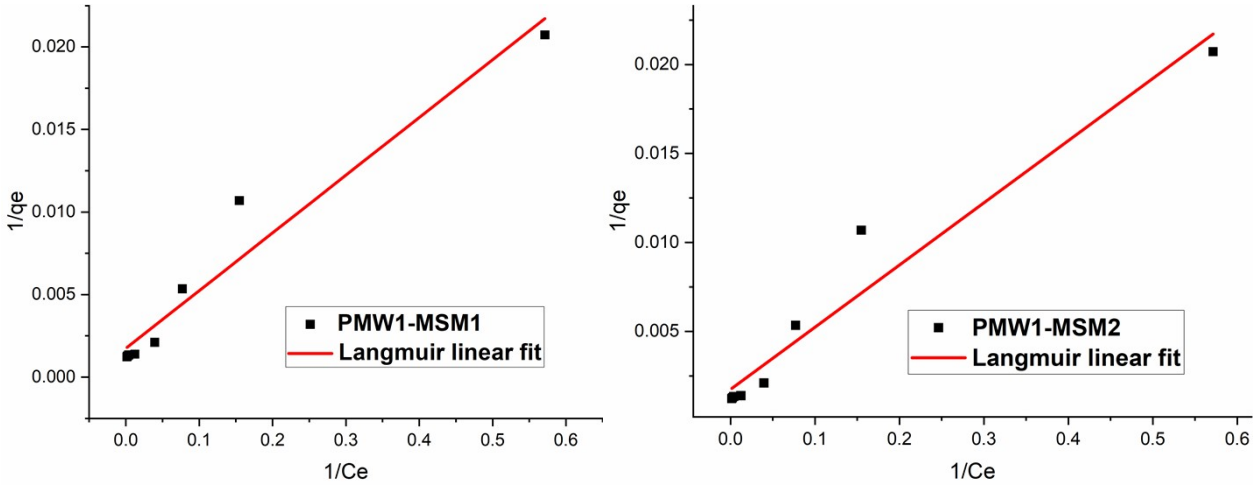

Fig. S28. Adsorption isotherm fitting for Pb(II) adsorption on PMW1-MSM1 and PMW1-MSM2 at 25°C using linear Langmuir model.

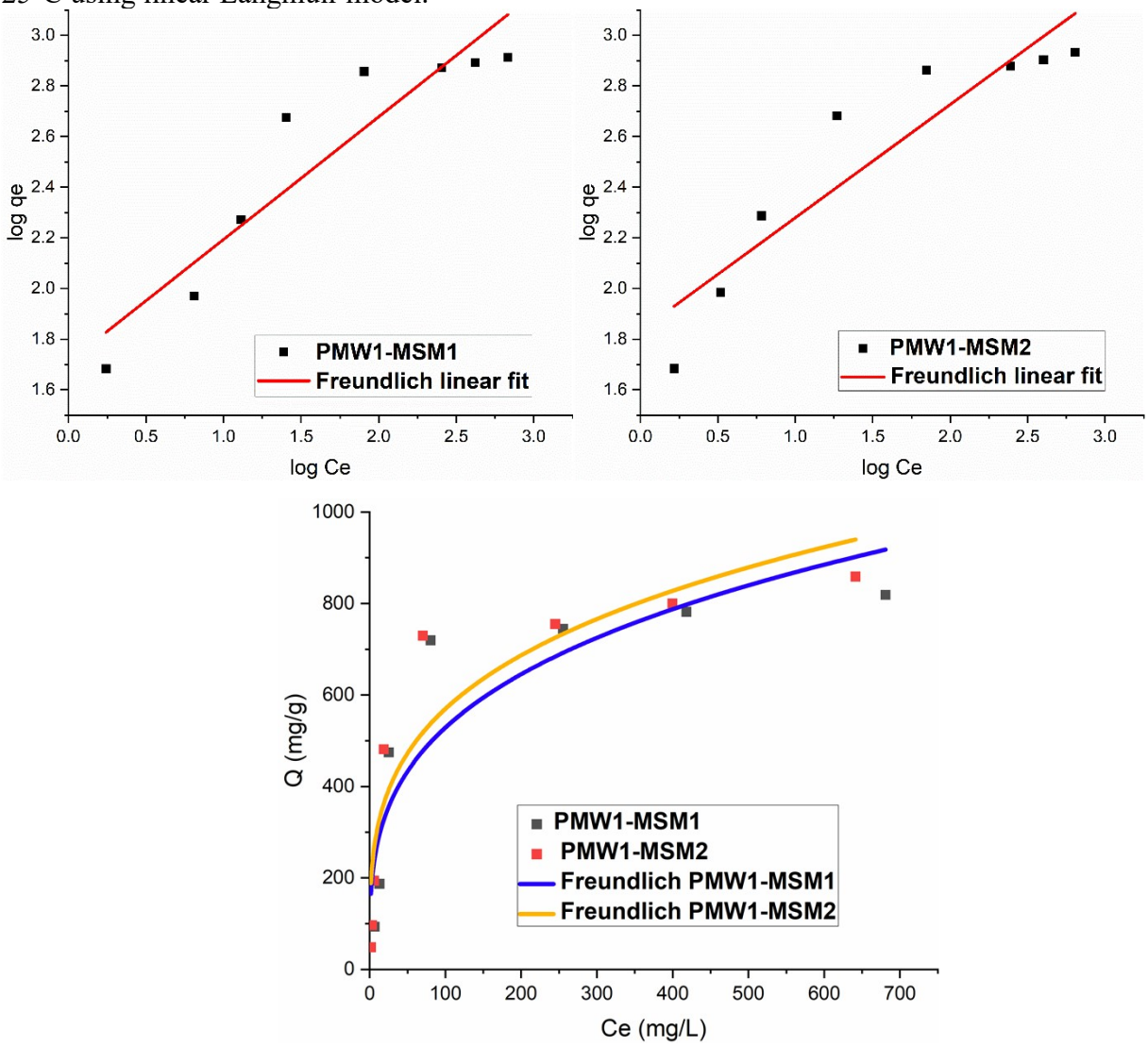

Fig. S29. Adsorption isotherm fitting for Pb(II) adsorption on PMW1-MSM1 and PMW1-MSM2 at 25°C using different linear and nonlinear Freundlich models.

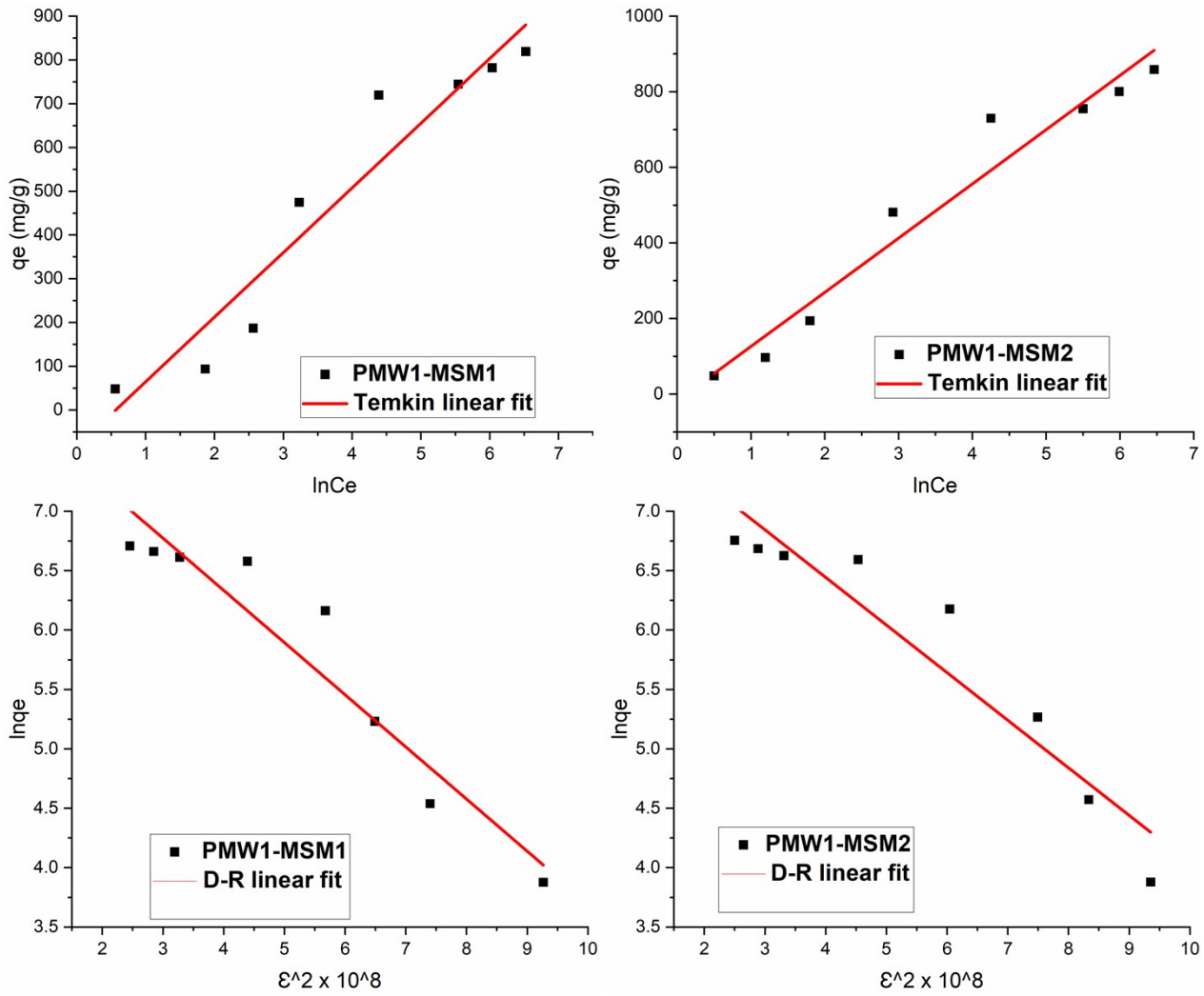

Fig. S30. Adsorption isotherm fitting for Pb(II) adsorption on PMW1-MSM1 and PMW1-MSM2 at 25°C using Temkin model and Dubinin-Radushkevich models.

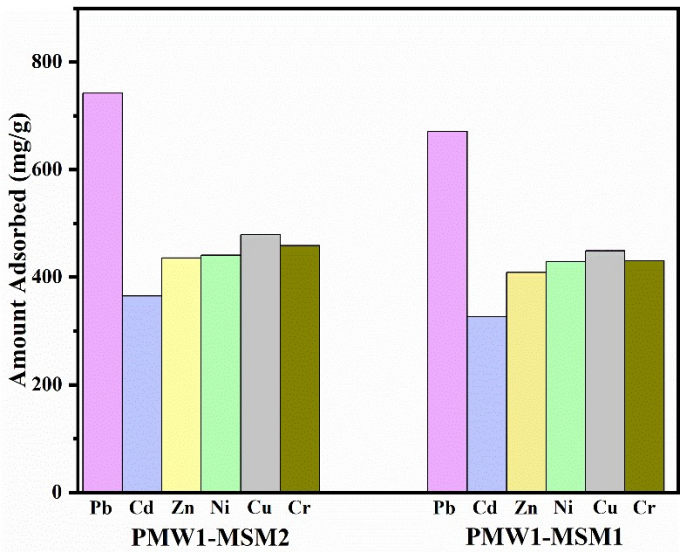

Fig. S31. Effect of competing metal ions on Pb(II) removal efficiency by the MSMs.

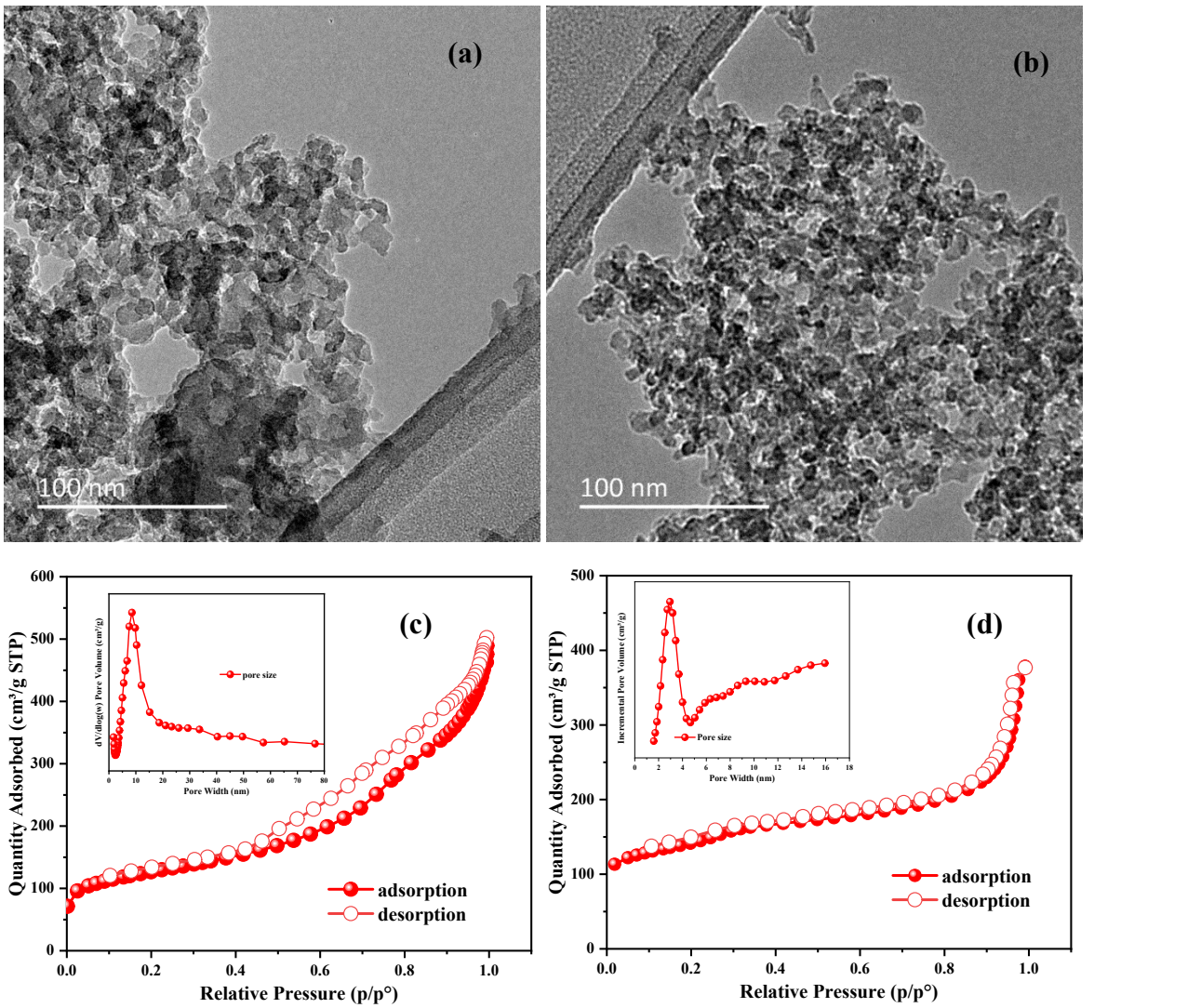

Fig. S32. TEM and N_2 sorption analysis of the adsorbents after four adsorption-desorption cycles: TEM micrographs of PMW1-MSM1 (a) and PMW1-MSM2 (b); N_2 sorption analysis of PMW1-MSM1 (c) and PMW1-MSM2 (d).

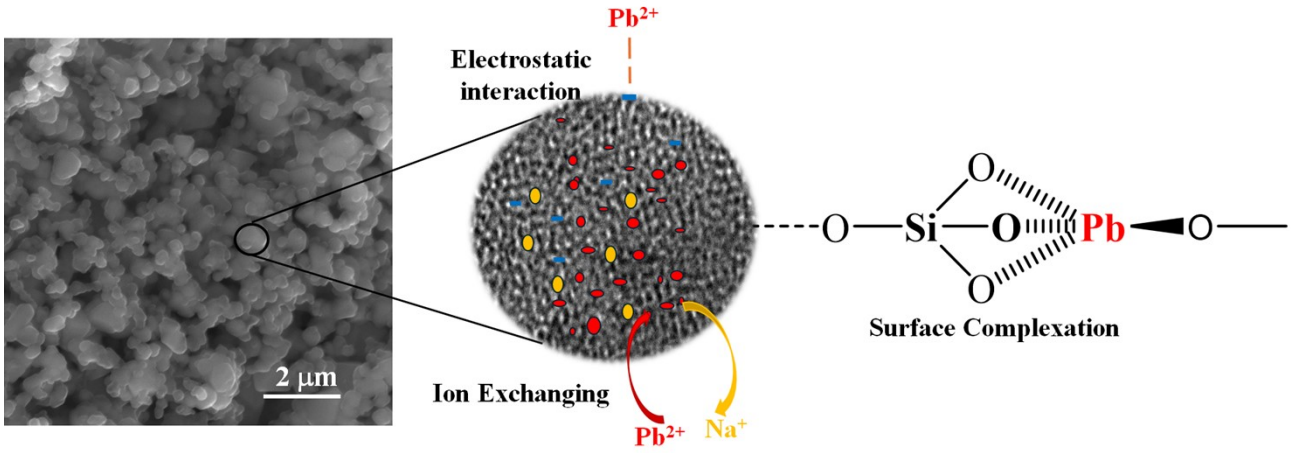

Fig. S33. Proposed mechanism the Pb(II)-adsorbent interaction.

3. Supplementary Tables

Table S1. Summary of surface area, pore size and pore volume of hetero-functional porous materials synthesized from PMW precursors.

Sample	BET surface area (m^2/g)	Pore size (nm)	Pore volume (cm^3/g) at $P/P_0 = 0.98$
PMW1	35	-	-
PMW2	12	-	-
PMW1-MSM1	659	4-18 (12)	1.39
PMW1-MSM2	954	2-3.1 (2.5)	0.94
PMW2-MSM3	577	6-16 (9.1)	0.69
PMW2-MSM4	780	2-3.2 (2.4)	0.42

Table S2. Pb^{2+} adsorption kinetic parameters using the pseudo-first order, pseudo-second-order, and intraparticle diffusion kinetic models onto MSMs.

Kinetics	Equation	Linear plot	Parameters	Values (PMW1-MSM1)	Values (PMW1-MSM2)
Pseudo-first-order	$\ln(q_e-q_t) = \ln q_e - K_1 t$	ln (qe-qt) *vs* t	k_1 (min^{-1})	0.003	0.009
			$q_{e(calc)}$ (mg/g)	5011.87	54954.09
			R^2	0.05	0.64
Pseudo-second-order	$\frac{t}{qt} = \frac{1}{K2{q_e}^2} + \frac{t}{q_e}$	t/qt vs t	k_2 (min^{-1})	0.00047	0.000258
			$q_{e(calc)}$ (mg/g)	813.008	869.565
			R^2	0.98836	0.99922
Intraparticle diffusion	$qt = k_{diff} t^{1/2} + C$	qt *vs* $t^{1/2}$	K_{diff} ($mg/g/min^{1/2}$)	7.76713	8.46164
			C (mg/g)	681.248	719.401
			R^2	0.33292	0.73666
Experimental data	-	-	$Qe_{(exp)}$ (mg/g)	826.72	869.33

qe = equilibrium adsorption capacity; qt = adsorption capacity at time t; t = time; K_1 = pseudo-first-order rate constant; K_2 = pseudo-second-order rate constant; k_{diff} = intraparticle diffusion rate constant; *C* = Intraparticle diffusion constant.

Table S3. Isotherm model parameters for the Pb^{2+} removal by MSMs.

Isotherm	Equation	Linear plot	Parameters	Values (PMW1-MSM1)	Values (PMW1-MSM2)
Langmuir (Nonlinear)	$q_e = (q_{max} \times KL \times C_e)$ $/(1 + KL \times C_e)$	q_{max} *vs* Ce	q_{max} (mg/g)	859.21	866.13
			K_L (L/mg)	35.57E+02	58.01E+02
			R^2	0.98	0.99
			Adj. R^2	0.97	0.99
Langmuir (Linear)	$\frac{1}{q_e} = \frac{1}{KLq_{max}} x \frac{1}{C_e} + \frac{1}{q_{max}}$	$\frac{1}{qe}$ *vs* $\frac{1}{Ce}$	q_{max} (mg/g)	5.75E+02	1.26E+03
			K_L (L/mg)	4.98E-02	2.47E-02
			R^2	0.94213	0.99398
			R_L	0.1672648-0.0386209	0.02631-0.44771
Freundlich (Linear)	$\ln q_e = \ln K_F + \frac{1}{n}(\ln C_e)$	$\ln q_e$ *vs* $\ln C_e$	K_F (mg/g) (L/mg) 1/ *n*	51.24010	68.0487
			n	2.0641	2.23748
			1/n	0.48447	4.47E-01
			R^2	0.85072	0.83359
Freundlich (Nonlinear)	$q_e = (q_{max} \times Kfr \times C_e)$ $/(1 + KL \times C_e)$	q_{max} *vs* Ce	K_{fr} (L/mg)	140.69	164.72
			n_{fr} (L/mg)	3.48	3.71
			R^2	0.83	0.86
			Adj. R^2	0.81	0.84
Temkin	$q_e = \frac{RT}{b_T} ln A_T +$ (RT/B_T) $ln C_e$	q_e *vs* $\ln C_e$	B_T (kJ/mol)	147.763	143.403
			A_T	0.56774	0.88479
			R^2	0.90904	0.94836
Dubnin-Radushkevich	$ln q_e = ln q_{max} - K_{DR}\varepsilon^2$ ($\varepsilon = RT \ln(1 + 1/C_e)$	$\ln q_e$ *vs* ε^2	q_{max} (mg/g)	3266.35	3122.50
			K_{DR} (mol^2/J^2)	4.39E-09	4.01E-09
			E (kJ/mol)	10.7	11.2
			R^2	0.90071	0.88987

qe = equilibrium adsorption capacity; q_{max}= maximum adsorption capacity; K_L=Langmuir constant; R_L=separation factor; R^2=correlation coefficient; K_F=Freundlich constant; n and 1/n= Freundlich heterogeneity constants; A_T and B_T= Temkin isotherm constant; Ɛ=Polanyi potential; K= Dubnin-Radushkevich constant; activity coefficient E=adsorption energy; T is the temperature (K); and *R* is the gas constant (J K^{-1} mol^{-1}).

Table S4. Zeta potentials of MSMs as a function of the pH in KCl (1 mM) solution.

PMW1-MSM1		PMW1-MSM2
pH	**Zeta P (mV)**	**Zeta P (mV)**
3	-27.3	-31.6
5	-27.3	-32.8
7	-34.7	-37.65
9	-42.7	-42.5
11	-45.5	-44.7

Table S5. Zeta potentials of MSMs as a function of Pb^{2+} concentration (b) in KCl (1 mM) solution.

Pb salt concentration (mg/)	PMW1-MSM1	PMW1-MSM2
	Zeta P (mV)	Zeta P (mV)
0	-34.7	-37.65
500	1.41	-1.35
1000	18.3	13.85
1500	27.45	29.3

Table S6. Lead (II) adsorption performances of various reported sorbents.

Adsorbent	BET Surface area (cm^2/g), Pore Volume (cm^3/g), Pore Size (nm)	Initial concentration of Pb(II) (mg/L)	Condition (time, pH)	Pb(II) uptake (mg/g)	Reference
PMW1-MSM1	768, 0.62, 11.2	0-1500	2 h, 7	830	This work
PMW1-MSM2	920, 0.80, 2.9	0-1500	2 h, 7	870	This work
Fe_3O_4@MIL-8A(Fe)/ APTMS	62, 9.4, 2.6	0-100	0.5 h, 7	536	[1]
UiO-66-NH_2-PAM-PET	13, - ,8	0.2-1.2	8 h, 5	712	[2]
Methylthiazole-Schiff base@SBA-15	214,0,4, 6.3	0-400	10 h, 2	283	[3]
Fe_3O_4@SBA-15-Gd	232, 0.8, 13	0.175	1h, 8	333	[4]
Bis-Schiff base@SBA-15	175,0.3, 4.9	10-300	15 h, 6	152	[5]
Thiazole-Schiff base@SBA-15	192, 0.4, 4.8	0-200	24 h, 6	149	[6]
MCM-41	-	0-10	0.6 h, 4.5	132	[7]
$ZnCl_2$@MCM-41	754, 0.58, 2.8	2-200	1 h, 7	479	[8]
Calcium Alginate@ SBA-15	33.22, 0.04, 3.72	50-1000	3.3 h, 7	1029	[9]
EDTA@SBA-15	284, 0.5, 7.16	0-100	0.3 h, 5	273	[10]
Salen@MCM-41	8, 0.05, -	0-100	2h, 5.5	139	[11]
Functionalized-A-MOF	255, 0.117,8	0-200	5 h, 3.5	366	[12]
ZIF-8	-	0-100	0.5 h, 7	455	[13]
Graphene Oxide@ZIF-8	-	0-500	0.2 h, 5.5	556	[14]
Zeolite NaA	12.4, - 0.9	0-200	0.3 h, 5	488	[15]
MNPs-SBA-15-Met	325, 0.4, 5.4	10-400	2 h, 4.8	272	[16]
hydroxyphosphatoethyl-MSM	325, 0.4, 5.4	0-300	2 h, 4.8	272	[17]

Table S7. Weight percentages of primary chemical constituents for the synthesis of PMW-based MSMs as determined by SEM-EDX analysis

Element	**PMW1-MSM1**	**PMW1-MSM2**	**PMW2-MSM3**	**PMW2-MSM4**
Aluminum (Wt. %)	0.19	0.84	0.38	0.77
Oxygen (Wt. %)	82.46	83.23	73.78	76.98
Silicon (Wt. %)	15.89	14.78	24.37	21.43
Sodium (Wt. %)	1.46	1.88	1.48	2.33
Mass of SiO_2(g)	~0.58	~0.51	~0.69	~0.66
Mass of Al_2O_3(g)	~0.01	~0.03	~0.01	~0.02

Table S8. Average precursor cost for preparing a kg of MCM-41 and SBA-15 via conventional routes from analytical grade reagents.

Chemical Name	**Chemical formula**	**Quantity estimated (in kg) to produce 1 kg MSM**	**Average unit price from commercial vendors**	**Approximate price to prepare 1kg MSM**	**Cost Benefit***
Tetramethylammonium silicate solution	$(CH_3)_4N(OH)\cdot 2SiO_2$	1.49	$310/kg	$462	559-(5.85 x 40) = $325
Sodium silicate	$Na_2O(SiO_2)x\cdot xH_2O$	0.78	$ 15/kg	$12	
CAB-0-SIL M-5 (Fumed silica)	SiO_2	0.74	$115/kg	$85	
Tetraethyl orthosilicate	$Si(OC_2H_5)_4$	3.87	$80/kg	$310	310-(6.17 x 40) = $63
Sodium hydroxide	NaOH		$40/kg	$7.10/kg	

* Obtained by subtracting NaOH cost to produce 1 kg of the corresponding PMW-based MSM from the total silica source cost.

Table S9. Thermodynamic parameters for PMW1-MSM1 and PMW1-MSM2.

Sample	**Temperature (℃)**	lnK_c	**Thermodynamic parameters**		
			ΔH° (kJ/mol)	ΔS° (J mol/K)	ΔG° (kJ/mol)
PMW1-MSM1	25	1.07	3.01	19.09	-2.65
	35	1.15			-2.95
	45	1.16			-3.07
	55	1.19			-3.24
PMW1-MSM2	25	1.13	3.23	20.31	-2.79
	35	1.20			-3.06
	45	1.23			-3.24
	55	1.25			-3.41

References

1. M. E. Mahmoud, M. F. Amira, S. M. Seleim and A. K. Mohamed, *J. Hazard. Mater.*, 2020, **381**, 120979.
2. F. Zhao, C. Su, W. Yang, Y. Han, X. Luo, C. Li, W. Tang, T. Yue and Z. Li, *Appl. Surf. Sci.*, 2020, **527**, 146862.
3. H. Liang, K. Chai, F. Shen, H. He, G. He, C. Chen and Z. Wei, *Microporous Mesoporous Mater.*, 2023, **351**, 112476.
4. F. Hassanzadeh-Afruzi, F. Esmailzadeh, S. Asgharnasl, F. Ganjali, R. Taheri-Ledari and A. Maleki, *Sep. Purif. Technol.*, 2022, **291**, 120956.
5. L. Zheng, Y. Yang, Y. Zhang, T. Zhu and X. Wang, *J. Solid State Chem.*, 2021, **301**, 122320.
6. W. Wang, G. Wu, T. Zhu, Y. Yang and Y. Zhang, *J. Taiwan Inst. Chem. Eng.*, 2021, **125**, 349-359.
7. X.-D. Li and Q.-Z. Zhai, *Appl. Water Sci.*, 2020, **10**, 122.
8. F. Raji, A. Saraeian, M. Pakizeh and F. Attarzadeh, *RSC Adv.*, 2015, **5**, 37066-37077.
9. Y. Song, L.-Y. Yang, Y.-g. Wang, D. Yu, J. Shen and X.-k. Ouyang, *Int. J. Biol. Macromol.*, 2019, **125**, 808-819.
10. J. Huang, M. Ye, Y. Qu, L. Chu, R. Chen, Q. He and D. Xu, *J. Colloid Interface Sci.*, 2012, **385**, 137-146.
11. D. F. Enache, E. Vasile, C. M. Simonescu, D. Culita, E. Vasile, O. Oprea, A. M. Pandele, A. Razvan, F. Dumitru and G. Nechifor, *RSC Adv.*, 2018, **8**, 176-189.
12. H. Wang, S. Wang, S. Wang, L. Fu and L. Zhang, *J. Environ. Chem. Eng.*, 2023, **11**, 109335.
13. S. Z. N. Ahmad, W. N. W. Salleh, N. Yusof, M. Z. M. Yusop, R. Hamdan and A. F. Ismail, *Appl. Nanosci.*, 2023, **13**, 4005-4019.
14. S. Z. N. Ahmad, W. N. W. Salleh, M. Z. M. Yusop, R. Hamdan, F. Aziz, N. A. Awang and A. F. Ismail, *J. Chem. Technol. Biotechnol.* , 2023, **98**, 2668-2676.
15. Y. Lv, B. Ma, Y. Liu, C. Wang and Y. Chen, *Microporous Mesoporous Mater.*, 2022, **329**, 111553.
16. S. Shahabuddin, C. Tashakori, M. A. Kamboh, Z. Sotoudehnia Korrani, R. Saidur, H. Rashidi Nodeh and M. E. Bidhendi, *Environ. Sci.: Water Res. Technol*, 2018, **4**, 549-558.

17. C. Gunathilake, M. S. Kadanapitiye, O. Dudarko, S. D. Huang and M. Jaroniec, *ACS Appl. Mater. Interfaces*, 2015, **7**, 23144-23152.